analytical chemistry

Letter

pubs.acs.org/ac

Single-Cell-Kinetics Approach to Discover Functionally Distinct Subpopulations within Phenotypically Uniform Populations of Cells

Vasilij Koshkin and Sergey N. Krylov*

Department of Chemistry and Centre for Research on Biomolecular Interactions, York University, Toronto, Ontario M3J 1P3, Canada

Supporting Information

ABSTRACT: Phenotypically uniform cell populations may contain subpopulations with different activities of enzymes, membrane transporters, and other functional units which can be characterized kinetically. Here we propose the first approach to the discovery of such subpopulations; we term it single-cell approach to discover subpopulations or SCADS for short. SCADS combines microscopy, single-cell kinetic analysis, and population/cluster analysis to discover a functionally distinct subpopulation of cells. In this proof-of-principle work, we used SCADS to search for subpopulations with distinct kinetic patterns of membrane transport in bulk tumor cells (BTCs) and tumor-initiating cells (TICs). We used two classical Michaelis parameters, V_{max} and K_M, to kinetically characterize the rate of transport. We found that the BTC population was homogeneous with respect to membrane transport. When analyzing TICs, we discovered three main functionally distinct subpopulations: (i) cells with a high rate of transport (high V_{max}), (ii) cells with high-affinity transporters (low K_M), and (iii) cells with activity and affinity similar to those in BTCs (low V_{max} and high K_M).

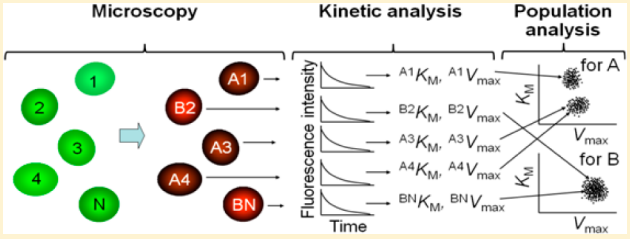

Understanding molecular mechanisms that govern embryogenesis, carcinogenesis, and tissue regeneration requires the classification of highly heterogeneous cells into populations with uniform properties.[1] For example, cancerous cells can be split into two major populations: tumor-initiating cells (TICs) and bulk tumor cells (BTCs).[2] Stem cells can also be roughly classified into two populations: cycling stem cells and dormant stem cells.[3]

Cell heterogeneity is typically determined through proteomic and genomic-based analyses. For example, fluorescent antibodies against cell-surface markers, such as CD44, CD24, EpCAM, etc., are used to group cells into phenotypically uniform populations.[4] It is well appreciated that phenotypically uniform cell populations may contain multiple levels of functionally distinct subpopulations that cannot be identified with known cell-surface markers.[5] Also cellular functioning is often governed by parameters which are difficult or impossible to characterize in proteomic or genomic screening, such as the composition and fluidity of the cell membranes. Hence, the discovery of functionally distinct subpopulations of cells within phenotypically uniform populations is very challenging.

Many cellular functions, e.g., activities of enzymes and membrane transporters can be characterized kinetically.[6] Microscopy-based assays utilizing fluorescent and fluorogenic substrates have been developed for the kinetic characterization of cells.[7] However, there is still no approach available for the discovery of kinetically distinct subpopulations of cells within phenotypically uniform populations. Here we introduce such an approach which combines microscopy, kinetic analysis, and population analysis. The approach is termed single-cell approach to discover subpopulations, or SCADS for short, and is conceptually depicted in Figure 1. In step 1, all cells are loaded with a fluorescent (fluorogenic) substrate that will be used to visually assess the cells functional activity. Time-lapse microscopy is utilized to follow the kinetics of substrate-to-product conversion in individual cells. In step 2, all cells are stained using fluorescently labeled antibodies which target specific cell-surface markers. Microscopy is used to visualize

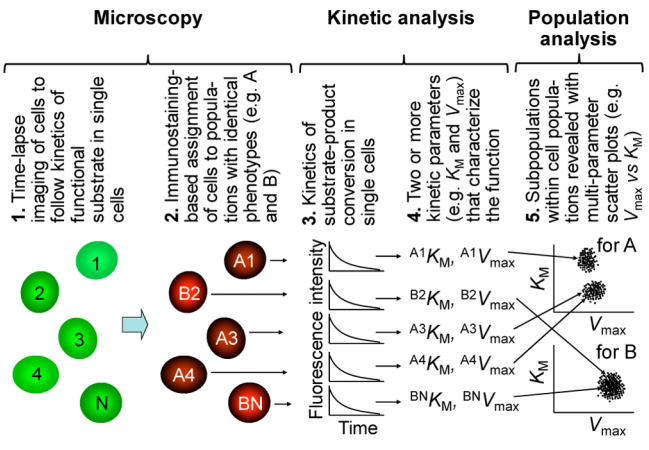

Figure 1. Schematic illustration of single-cell-kinetics approach to discover functionally distinct subpopulations within phenotypically uniform populations of cells. See text for details.

Received: January 15, 2013
Accepted: February 10, 2013
Published: February 11, 2013

   dx.doi.org/10.1021/ac400151v | *Anal. Chem.* 2013, 85, 2578−2581

antibody staining and assign cells to phenotypically uniform populations. In step 3, individual kinetic traces characterizing the substrates conversion into product are built for each cell. In step 4, the kinetic traces are used to measure specific kinetic parameters, such as K_M and V_{max}, for every cell. Finally, in step 5 of SCADS, these kinetic parameters are plotted on a separate scatter graph for every phenotypically unique population, and cluster analysis is used to group the cells into functionally distinct subpopulations. In this proof-of-principle work, we applied SCADS to search for subpopulations with different kinetics of membrane transport associated with multidrug-resistance (MDR) in BTCs and TICs. We found that the BTC population was homogeneous and contained only cells with low V_{max} and high K_M. In the TIC population, we discovered three functionally distinct subpopulations: (i) cells with high V_{max} (high flux), (ii) cells with low K_M (high affinity), and (iii) cells similar to BTCs (low flux, low affinity).

Tumors consist of two major cell types, BTCs and TICs, which differ considerably in their functions.[8] TICs represent a very small population of tumor cells which are responsible for the formation and dissemination of tumors as well as for tumor resistance to therapies. BTCs are all the remaining tumor cells. One of the main reasons for failure of cancer chemotherapies is the elevated multidrug resistance (MDR) found in TICs, i.e., the increased ability to expel drugs from the cell interior.[9] High MDR capacity of the TIC population is driven by membrane transporters of the ABC (ATP binding cassette) superfamily.[10] Accordingly, we applied our SCADS approach to look for subpopulations with different MDR capabilities in BTCs and TICs. Cultured breast cancer cells (MCF-7) were used as an experimental model, since the TIC population in this cell line is well characterized.[11]

Below we outline the essence of the experimental procedures and data analysis used in this study (see the Supporting Information and ref 12 for details). TICs typically constitute a small fraction of cancerous cell population (often less than 1%).[11] To analyze a statistically significant number of TICs, a cell population enriched with TICs must be obtained. The enrichment was achieved by the anchorage-independent culturing of cells as floating tumorspheres.[13] The cells which grow as regular monolayers are virtually 100% BTCs. We used regular monolayers to derive populations that could serve as a BTC control. In contrast, dispersed tumorspheres contain not only BTCs but also TICs (10−50%).[13] Accordingly, cell populations derived from the dispersed tumorspheres were used for the analysis of both BTCs and TICs. The cells isolated from the dispersed tumorspheres were cultured in an anchored state for 2−3 days to reach 50−60% confluence. They were loaded with fluorescein, a fluorescent MDR substrate, by adding it to the cell media and incubating for 0.5 h.[14] Our recent experiments determined that fluorescein is the only actively transported MDR substrate in naive (not exposed to chemotherapy) MCF-7 cells.[12] The cells were then allowed to expel the substrate by removing it from the media. Previous work with this type of cells has demonstrated only an insignificant contribution of ABC transporter-independent diffusion to the overall fluorescein efflux.[12] Time-lapse microscopy images were taken at 5-min intervals for 2−3 h. After the fluorescein exclusion was completed, the cells were fixed, treated with the primary antibodies against CD44 and CD24, followed by incubation with the fluorescently labeled secondary antibodies. Multiple (4−9) fluorescent images were taken (at 530 and 665 nm for the FITC- and PE/Cy5-labeled secondary antibodies, respectively). The images were averaged to increase the signal-to-noise ratio for the reliable assessment of marker expression levels in individual cells. This approach is similar to image-based immunophenotyping that is used when flow cytometry is not applicable.[15,16] The following steps were performed during data analysis. First, a combination of high CD44 expression and low CD24 expression was used as a molecular signature in order to identify the TICs in the cultured breast cancer cells.[17] The remaining cells were assigned to BTCs. The kinetics of fluorescein efflux from individual cells were fitted to an integrated Michaelis−Menten equation to find the corresponding K_M and V_{max} values of MDR-associated transport. Scatter plots of K_M versus V_{max} were used to analyze TIC and BTC populations. Visual analysis of clusters on the scatter plots along with statistical treatment (*k*-means clustering, STATISTICA software) were finally used to identify subpopulations of cells with different MDR activities. The ability to follow the cell's fate throughout the entire experiment is pivotal to SCADS. Therefore, all the measurements were performed on cells anchored to gridded culture dishes.

The typical time course of fluorescein efflux is illustrated in Figure 2A. Figure 2B depicts the same cells following the immunostaining treatment. Our images of CD44/CD24 staining were similar to those obtained for this type of cells without preceding MDR kinetics measurements,[18,19] which confirms that MDR measurements did not significantly affect CD44/CD24 staining. The cells that exhibited high red fluorescence (high CD44) and low green fluorescence (low CD24) were assigned to TICs while the remaining cells were assigned to BTCs. Figure 2C shows 2 TICs and 7 BTCs for the

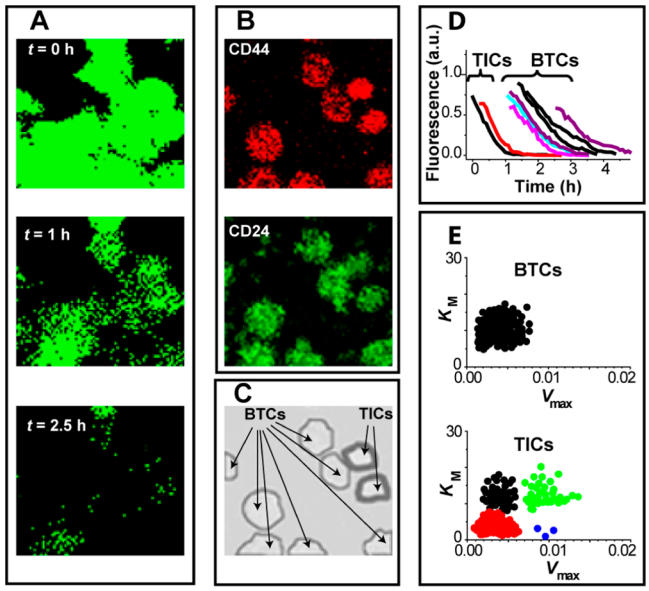

Figure 2. Application of the SCADS approach to discover cell subpopulations with different MDR activity in breast BTCs and TICs. Panel A illustrates progressive MDR-associated efflux of fluorescein from cells. Panel B depicts images of the cells shown in panel A but after immunostaining with CD44 and CD24 antibodies. Panel C shows TICs and BTCs identified based on the images depicted in panel B. Panel D illustrates kinetic traces of MDR-associated efflux of fluorescein from the cells shown in the previous images. Panel E shows cumulative scatter plots of Michaelis parameters derived from the MDR kinetics (such as those in panel D) for BTCs and TICs using the data for a total of 488 cells.

dx.doi.org/10.1021/ac400151v | *Anal. Chem.* 2013, 85, 2578−2581

image presented in Figures 2A,B. Overall, we analyzed 244 TICs population and 244 BTCs.

The time-lapse microscopy data was used to plot kinetics of fluorescein efflux for all the cells analyzed. Figure 2D shows examples of kinetic traces obtained for each individual cell depicted in Figure 2A−C. All kinetic traces were individually fitted with the Michaelis−Menten equation to find K_M and V_{max} for every cell. Finally, we examined if phenotypically defined TIC and BTC populations contained subpopulations with kinetically different MDR capacities. K_M versus V_{max} scatter plots were built for TICs and BTCs (Figure 2E). The BTC population does not exhibit noticeable heterogeneity; the cells form a single K_M versus V_{max} cluster. The situation is much more intriguing for TICs. Even the visual inspection of the plot clearly indicates the heterogeneous nature of the TIC population. Subsequent statistical analysis by *k*-means clustering confirmed the TICs heterogeneity with the ratio between intercluster and intracluster variability of 5−50-fold. We thus proved that SCADS can identify kinetically distinct subpopulations within phenotypically homogeneous cell populations.

While in this work we are mainly reporting the new method for subpopulation discovery, the physiological consequences of the discovered kinetic heterogeneity in TICs are of great importance and deserve some discussion. The cluster analysis of data in Figure 2E indicates that the TIC population includes three main subpopulations with distinct kinetics of MDR transport. The first subpopulation (green dots) represents cells with high V_{max} values. The second subpopulation (red dots) includes cells with low K_M values. The third subpopulation (black dots) consists of cells with both V_{max} and K_M identical to those in the BTC population (low V_{max} and high K_M). Mean values of V_{max} and K_M for the three subpopulations are given in Table S1 in the Supporting Information. There was the fourth subpopulation (blue dots) with both high V_{max} and low K_M, but its size (3 cells out of 488) was statistically insignificant for consideration in this work. The activation of MDR in TICs is thus mainly carried out either through the catalytic mechanism (increased flux) or through the binding mechanism (increased affinity) but not through both. The previously performed theoretical analysis of transmembrane drug equilibration suggests that both the increase in V_{max} and decrease in K_M of MDR transport should improve drug resistance in cancer cells.[20] Thus, the TIC subpopulations with increased V_{max} and decreased K_M can be expected to have greater drug resistance. The subpopulation with low V_{max} and high K_M might either constitute a specific subpopulation of TICs or reflect experimental errors in TIC identification based on CD44/CD24 staining.

The presence of a subpopulation with decreased K_M is potentially a less general feature of TICs than a subpopulation with increased V_{max}. It is known that a modification in ABC transporters may improve their specific affinity to some substrates but worsen their affinity to others.[21] Thus, instead of simple MDR activation in TICs, one can expect more complex distinctions between MDR in TICs and BTCs. In other words, MDR transporters in TICs may provide better cell protection for some anticancer drugs but unchanged or worsened protection for others. This could explain recent reports which are inconsistent with broadly accepted activation of MDR in TICs.[22]

In addition, the TICs subpopulation with high MDR affinity may cause specific therapeutic consequences. It is conceivable that a reduced K_M in TICs may give the cells a selective advantage in the case of metronomic chemotherapy.[23] The metronomic chemotherapy is the application of chemotherapeutics in low doses to minimize their toxic effects. The low doses are believed to help avoid prolonged drug-free breaks between periods of drug administration and, therefore, reduce the chance of tumor relapse. The presence of TIC subpopulations with low K_M can potentially have the following effect. At high drug doses (conventional chemotherapy), MDR transporters in BTCs (high K_M) and TICs (low K_M) will both be saturated and function at their maximal rates. At low doses (metronomic chemotherapy), the low-K_M transporters in TICs may remain saturated, while the transporters in BTCs are already not saturated and thus poorly efficient. This will lead to the preferential survival of TICs during the metronomic treatment regimens, which is highly undesirable. Therefore, the SCADS-based testing of tumor samples for MDR affinity can allow rational planning of a therapeutic strategy.

Integrated analyses of functional and phenotypic cellular features attract growing attention since they promise multifaceted description of cell functioning.[5] Until now the evaluation of functional parameters was accomplished with single-step "end-point" methods, which suffer from a number of inherent limitations.[24] Here we estimate cells' function using a kinetic approach, which provides two parameters (V_{max} and K_M) instead of the one parameter obtained with the end-point methods. This extra information gives deeper insights into the mechanisms and consequences of the observed cellular alterations. In particular, the modulations of MDR affinity in TIC subpopulations discovered here are expected to affect tumor response to treatment and, thus, therapeutic strategy. To conclude, we foresee wide use of the SCADS approach in basic research and in clinical applications, specifically in oncology. The practical use of SCADS will obviously require high-throughput microscopy techniques with automated image analysis.[25]

■ ASSOCIATED CONTENT

Ⓢ Supporting Information

Supporting materials and methods and supporting table. This material is available free of charge via the Internet at http://pubs.acs.org.

■ AUTHOR INFORMATION

Corresponding Author

*E-mail: skrylov@yorku.ca.

Notes

The authors declare no competing financial interest.

■ ACKNOWLEDGMENTS

The work was funded by NSERC Canada.

■ REFERENCES

(1) Liu, X.; Long, F.; Peng, H.; Aerni, S. J.; Jiang, M.; Sanchez-Blanco, A.; Murray, J. I.; Preston, E.; Mericle, B.; Batzoglou, S.; Myers, E. W.; Kim, S. K. *Cell* **2009**, *139*, 623−633.

(2) Ailles, L. E.; Weissman, I. L. *Curr. Opin. Biotechnol.* **2007**, *18*, 460−466.

(3) Raaijmakers, M. H.; Scadden, D. T. *Cell* **2008**, *135*, 1006−1008.

(4) Wang, D.; Bodovitz, S. *Trends Biotechnol.* **2010**, *28*, 281−290.

(5) (a) Golding, H.; Mizuochi, T.; McCarthy, S. A.; Cleveland, C. A.; Singer, A. *J. Immunol.* **1987**, *138*, 10−17. (b) Seita, J.; Asakawa, M.; Ooehara, J.; Takayanagi, S.; Morita, Y.; Watanabe, N.; Fujita, K.; Kudo, M.; Mizuguchi, J.; Ema, H.; Nakauchi, H.; Yoshimoto, T. *Blood* **2008**,

111, 1903−1912. (c) Park, T.; Monzo, H.; Mee, E. W.; Bergin, P. S.; Teoh, H. H.; Montgomery, J. M.; Faull, R. L. M.; Curtis, M. A.; Dragunow, M. *PLoS One* **2012**, *7*, e37742. (d) Challen, G. A.; Boles, N. C.; Chambers, S. M.; Goodell, M. A. *Cell Stem Cell* **2010**, *6*, 265−278.
(6) Gutfreund, H. *Kinetics for the Life Sciences*; Cambridge University Press: Cambridge, U.K., 1998; pp 3−10.
(7) Solis, E., Jr.; Zdravkovic, I.; Tomlinson, I. D.; Noskov, S. Y.; Rosenthal, S. J.; De Felice, L. J. *J. Biol. Chem.* **2012**, *287*, 8852−8863.
(8) (a) Lee, J. T.; Herlyn, M. *J. Cell. Physiol.* **2007**, *213*, 603−609. (b) Bansal, N.; Banerjee, D. *Curr. Pharm. Biotechnol.* **2009**, *10*, 192−196.
(9) Boumendjel, A., Bouttonat, J., Robert, J., Eds. *ABC Transporters and Multidrug Resistance*; John Wiley & Sons: Hoboken, NJ, 2009.
(10) Rees, D. C.; Johnson, E.; Lewinson, O. *Nat. Rev. Mol. Cell Biol.* **2009**, *10*, 218−227.
(11) (a) Engelmann, K.; Shen, H.; Finn, O. J. *Cancer Res.* **2008**, *68*, 2419−2426. (b) Karimi-Busheri, F.; Rasouli-Nia, A.; Mackey, J. R.; Weinfeld, M. *Breast Cancer Res.* **2010**, *12*, R31.
(12) Koshkin, V.; Krylov, S. N. *PLoS One* **2012**, *7*, e41368.
(13) (a) Ponti, D.; Costa, A.; Zaffaroni, N.; Pratesi, G.; Petrangolini, G.; Coradini, D.; Pilotti, S.; Pierotti, M. A.; Daidone, M. G. *Cancer Res.* **2005**, *65*, 5506−5511. (b) Cioce, M.; Gherardi, S.; Viglietto, G.; Strano, S.; Blandino, G.; Muti, P.; Ciliberto, G. *Cell Cycle* **2010**, *9*, 2878−2887.
(14) Sun, H.; Johnson, D. R.; Finch, R. A.; Sartorelli, A. C.; Miller, D. W.; Elmquist, W. F. *Biochem. Biophys. Res. Commun.* **2001**, *284*, 863−869.
(15) (a) Goodale, D.; Phay, C.; Postenka, C. O.; Keeney, M.; Allan, A. L. *Cytometry A* **2009**, *75*, 344−355. (b) Oswald, J.; Jørgensen, B.; Pompe, T.; Kobe, F.; Salchert, K.; Bornhäuser, M.; Ehninger, G.; Werner, C. *Cytometry A* **2004**, *57*, 100−107.
(16) Chan, L. L.; Zhong, X.; Qiu, J.; Li, P. Y.; Lin, B. *Cytometry A* **2011**, *79*, 507−517.
(17) Iliopoulos, D.; Hirsch, H. A.; Wang, G.; Struhl, K. *Proc. Natl. Acad. Sci. U.S.A.* **2011**, *108*, 1397−1402.
(18) Theodoropoulos, P. A.; Polioudaki, H.; Agelaki, S.; Kallergi, G.; Saridaki, Z.; Mavroudis, D.; Georgoulias, V. *Cancer Lett.* **2010**, *288*, 99−106.
(19) Oliveras-Ferraros, C.; Vazquez-Martin, A.; Martin-Castillo, B.; Cufí, S.; Del Barco, S.; Lopez-Bonet, E.; Brunet, J.; Menendez, J. A. *Biochem. Biophys. Res. Commun.* **2010**, *397*, 27−33.
(20) Stein, W. D. *Physiol. Rev.* **1997**, *77*, 545−590.
(21) Eckford, P. D.; Sharom, F. J. *Biochemistry* **2008**, *47*, 13686−13698.
(22) (a) Aulmann, S.; Waldburger, N.; Penzel, R.; Andrulis, M.; Schirmacher, P.; Sinn, H. P. *Hum. Pathol.* **2010**, *41*, 574−581. (b) Yan, H.; Chen, X.; Zhang, Q.; Qin, J.; Li, H.; Liu, C.; Calhoun-Davis, T.; Coletta, L. D.; Klostergaard, J.; Fokt, I.; Skora, S.; Priebe, W.; Bi, Y.; Tang, D. G. *PLoS One* **2011**, *6*, e24397.
(23) (a) Scharovsky, O. G.; Mainetti, L. E.; Rozados, V. R. *Curr. Oncol.* **2009**, *16*, 7−15. (b) Pasquier, E.; Kavallaris, M.; André, N. *Nat. Rev. Clin. Oncol.* **2010**, *7*, 455−465.
(24) Copeland, R. A. *Enzymes: A Practical Introduction to Structure, Mechanism, and Data Analysis*; VCH Publishers: New York, 1996; pp 124−125.
(25) Fero, M.; Pogliano, K. *Cold Spring Harb. Perspect. Biol.* **2010**, *2*, a000455.

SUPPORTING INFORMATION

Single-Cell-Kinetics Approach to Discover Functionally-Distinct Subpopulations within Phenotypically-Uniform Populations of Cells

Vasilij Koshkin and Sergey N. Krylov

Department of Chemistry and Centre for Research on Biomolecular Interactions, York University, Toronto, Ontario, M3J 1P3, Canada

Supporting Materials and Methods

Chemicals and materials. MCF-7 human breast cancer cells were purchased from the American Type Culture Collection (Manassas, VA, USA) and grown in monolayers as recommended by the supplier. To generate tumor spheres, the floating (loosely adherent) cells were collected by washing culture dishes at ~70% confluence.[1,2] Further cell culturing was performed in ultralow attachment plates (Corning, Acton, MA, USA) under serum-free conditions using medium #05621 with appropriate supplements developed by STEMCELL Technologies (Vancouver, BC, Canada). Cells were used within a culturing period of shorter than 6 months. Fluorescein was purchased from Sigma-Aldrich (St. Louis, MO), antibodies from Invitrogen (Carlsbad, CA), and all other reagents were obtained from Sigma-Aldrich (St. Louis, MO), Fluka AG (Buchs, Switzerland), or BDH Chemicals Ltd. (Poole, England).

Kinetic measurement of cell membrane transport. Cells at 50-60% confluence were loaded with the fluorescent MDR substrate, fluorescein, by incubating them in the media containing 5 μM fluorescein and 10 μM MDR inhibitor glyburide for 30 min at 37 ºC. The media was replaced with the fluorescein- and glyburide-free KRB buffer (115 mM NaCl, 5.9 mM KCl, 2.5 mM $CaCl_2$, 1.2 mM $MgCl_2$, 1.2 mM NaH_2PO_4, 15 mM $NaHCO_3$, 10 mM glucose, pH 7.4). Fluorescein efflux was monitored with a laser confocal scanner (Fluoview FV300, Olympus, Japan) at 5 min intervals for 2-3 h. Excitation at 488 nm was provided by an argon-ion laser, and emission was collected with the FITC filter set at 530 nm.

Phenotypic characterization of the cells. The cells were assessed for their CD44/CD24 status. After completing the MDR efflux assay described in the previous section, the cells were subjected to the immunophenotyping procedure (assessing quantity of CD44 and CD24 surface biomarkers) for discrimination between TICs and BTCs within the cell population located in the field of view. Immunostaining and imaging were based on established procedures as described by Gupta *et al.*,[3] except that FITC and PE/Cy5 were used as fluorescent labels instead of Alexa Fluo 488 and Alexa Fluo 555. Fluorescence images of fixed and antibody-treated cells were captured (with a fully open confocal aperture) at 530 and 665 nm using a confocal laser scanner FV300 (Olympus). Between 4 and 9 scans were collected and averaged to obtain an image with improved signal to noise ratio.

Data analysis. Single cell kinetics of MDR transport was described by progress curves of fluorescein efflux which were fitted to the integrated Michaelis-Menten equation for a single-substrate irreversible reaction:

$$V_{max}t = ([S]_0 - [S]) + K_M \ln([S]_0 / ([S]_0 - [S])$$

where $[S]_0$ and $[S]$ are the initial and current substrate concentrations, respectively.[4,5] Fitting was performed with Origin (Microcal Software, Northampton, MA) software.

Cell phenotypes were determined from fluorescence intensities of immunostained cells. Fluorescent cell images were quantified, and subjected to image-based cytometric analysis[6] for separation of BTC and TIC populations. To establish the gates to determine cell populations with high and low marker

expression, we used a well known fact that an MCF-7 cell monolayer culture has null or negligible content of TICs.[7,8]

Table S1: Mean Values of Michaelis Parameters for the homogenous BTC population and three TIC subpopulations

	V_{max}, nM/s	K_M, μM
BTC population	4.47 ± 0.39	10.02 ± 0.24
TIC subpopulation 1 (black dots in Fig. 2E)	3.96 ± 0.18	12.25 ± 0.43
TIC subpopulation 2 (green dots in Fig. 2E)	9.50 ± 0.28	12.59 ± 0.47
TIC subpopulation 3 (red dots in Fig. 2E)	3.32 ± 0.18	3.80 ± 0.24

Supporting References

1. Ponti, D.; Costa, A.; Zaffaroni, N.; Pratesi, G.; Petrangolini, G.; Coradini, D.; Pilotti, S.; Pierotti, M. A.; Daidone, M. G. *Cancer Res.* **2005**, *65*, 5506-5511.
2. Cioce, M.; Gherardi, S.; Viglietto, G.; Strano, S.; Blandino, G.; Muti P.; Ciliberto, G. *Cell Cycle* **2010**, *9*, 2878-2887.
3. Gupta, V.; Zhang, Q. J.; Liu, Y. Y. In: *Drug Design and Discovery: Methods and Protocols* Seetharama, D, Satyanarayanajois, D., Eds.; Methods in Molecular Biology; Humana Press: New York, NY, 2011; Vol. 716, pp. 179-191.
4. Duggleby, R. G. In: *Methods Enzymol*.; Purich, D.L., Ed; Academic Press: San Diego, CA, 1995; Vol. 249, pp. 61-90.
5. Stein, R. L.; Barbosa, M. D.; Bruckner, R. *Biochemistry* **2000**, *39*, 7973-7983.
6. Gerstner, A.O.H.; Mittag, A.; Laffers, W.; Dahnert, I.; Lenz, D.; Bootz, F.; Bocsi, J.; Tarnok, A. *J. Immunol. Methods* **2006**, *311*, 130-138.
7. Vesuna, F.; Lisok, A.; Kimble, B.; Raman, V. *Neoplasia* **2009**, *11*, 1318-1328.
8. Zhan, J. F.; Wu, L. P.; Chen L. H.; Yuan, Y. W.; Xie, G. Z.; Sun, A. M.; Liu, Y.; Chen, Z. X. *Cell Oncol. (Dordr).* **2011**, *34*, 451-456.